

REPORT DOCUMENTATION PAGE				Form Approved OMB NO. 0704-0188	
<p>The public reporting burden for this collection of information is estimated to average 1 hour per response, including the time for reviewing instructions, searching existing data sources, gathering and maintaining the data needed, and completing and reviewing the collection of information. Send comments regarding this burden estimate or any other aspect of this collection of information, including suggestions for reducing this burden, to Washington Headquarters Services, Directorate for Information Operations and Reports, 1215 Jefferson Davis Highway, Suite 1204, Arlington VA, 22202-4302. Respondents should be aware that notwithstanding any other provision of law, no person shall be subject to any penalty for failing to comply with a collection of information if it does not display a currently valid OMB control number.</p> <p>PLEASE DO NOT RETURN YOUR FORM TO THE ABOVE ADDRESS.</p>					
1. REPORT DATE (DD-MM-YYYY) 09-07-2013		2. REPORT TYPE Final Report		3. DATES COVERED (From - To) 1-Apr-2007 - 15-Dec-2012	
4. TITLE AND SUBTITLE Final Report			5a. CONTRACT NUMBER W911NF-07-1-0139		
			5b. GRANT NUMBER		
			5c. PROGRAM ELEMENT NUMBER 611102		
6. AUTHORS T. Alan Hatton			5d. PROJECT NUMBER		
			5e. TASK NUMBER		
			5f. WORK UNIT NUMBER		
7. PERFORMING ORGANIZATION NAMES AND ADDRESSES Massachusetts Institute of Technology (MIT) Office of Sponsored Programs 77 Massachusetts Avenue Cambridge, MA 02139 -4307				8. PERFORMING ORGANIZATION REPORT NUMBER	
9. SPONSORING/MONITORING AGENCY NAME(S) AND ADDRESS(ES) U.S. Army Research Office P.O. Box 12211 Research Triangle Park, NC 27709-2211				10. SPONSOR/MONITOR'S ACRONYM(S) ARO	
				11. SPONSOR/MONITOR'S REPORT NUMBER(S) 51972-CH.20	
12. DISTRIBUTION AVAILABILITY STATEMENT Approved for Public Release; Distribution Unlimited					
13. SUPPLEMENTARY NOTES The views, opinions and/or findings contained in this report are those of the author(s) and should not be construed as an official Department of the Army position, policy or decision, unless so designated by other documentation.					
14. ABSTRACT Porous inorganic or metal-organic materials with crystalline coordination structures and diverse topologies can be functionalized by inclusion of organic molecules. Specialized meso- and nanoporous matrices such as clays and metal-organic frameworks (MOF) possess sufficient mechanical, thermal, and chemical stability to yield promising materials when functionalized by organic ligands via inclusion of the ligands into the pores using supramolecular host-guest chemistry. Our work has focused on hybrid materials suitable for protection against organophosphorous					
15. SUBJECT TERMS nanoparticles, decontamination, recyclable, superparamagnetic					
16. SECURITY CLASSIFICATION OF:			17. LIMITATION OF ABSTRACT UU	15. NUMBER OF PAGES	19a. NAME OF RESPONSIBLE PERSON Trevor Hatton
a. REPORT UU	b. ABSTRACT UU	c. THIS PAGE UU			19b. TELEPHONE NUMBER 617-253-4588

## Report Title

Final Report

### ABSTRACT

Porous inorganic or metal-organic materials with crystalline coordination structures and diverse topologies can be functionalized by inclusion of organic molecules. Specialized meso- and nanoporous matrices such as clays and metal-organic frameworks (MOF) possess sufficient mechanical, thermal, and chemical stability to yield promising materials when functionalized by organic ligands via inclusion of the ligands into the pores using supramolecular host–guest chemistry. Our work has focused on hybrid materials suitable for protection against organophosphorous toxicants. Specifically, mesoporous matrices such as acidic montmorillonite K-10 and nanoporous chromium (III) terephthalate-based MOF (MIL-101) with multiple coordinatively unsaturated metal sites with Lewis acid properties were modified by inclusion of  $\pi$ -nucleophilic or supernucleophilic, basic ligand molecules such as 2-pralidoxime (PAM) and dimethylaminopyridine (DMAP), respectively. The resulting functionalized materials were effective in nucleophilic degradation of organophosphorous (OP) esters represented by CWA simulants and pesticides. Studies demonstrated that upon inclusion into the montmorillonite interlayer structure, the pyridinium group of sodium pralidoximate is strongly physisorbed onto acidic sites of the clay, leading to shrinking of the interplanar distance. Analogously, sorption of DMAP leads to changes in the MIL-101 structure, as demonstrated by X-ray diffractometry and FTIR. Degradation of diethyl parathion by the functionalized materials in aqueous-acetonitrile solutions occurred via hydrolytic conversion of parathion into diethylthio phosphoric acid, whereas hydrolytic degradation of diisopropyl fluorophosphate (DFP), a CWA simulant, was observed by  $^{31}\text{P}$  HRMAS to be rapid compared with these reactions in the untreated montmorillonite or MOF. The incorporation of the functionalized hybrid matrix particles into elastomeric film of polyisobutylene was shown to be a means to impart DFP-degrading capability to such films, which model chemically protective rubber gloves.

---

**Enter List of papers submitted or published that acknowledge ARO support from the start of the project to the date of this printing. List the papers, including journal references, in the following categories:**

**(a) Papers published in peer-reviewed journals (N/A for none)**

<u>Received</u>	<u>Paper</u>
-----------------	--------------

03/16/2009	1.00	Lev Bromberg, Heidi Schreuder-Gibson, William R. Creasy, David J. McGarvey, Roderick A. Fry, T. Alan Hatton. Degradation of Chemical Warfare Agents by Reactive Polymers, Industrial & Engineering Chemistry Research, (01 2009): . doi:
07/09/2013	18.00	Sa Wang, Lev Bromberg, Heidi Schreuder-Gibson, T. Alan Hatton. Organophosphorous Ester Degradation by Chromium(III) Terephthalate Metal–Organic Framework (MIL-101) Chelated to, ACS Applied Materials & Interfaces, (02 2013): 0. doi: 10.1021/am302359b
07/09/2013	19.00	Lev Bromberg, Christine M. Straut, Andrea Centrone, Eugene Wilusz, T. Alan Hatton. Montmorillonite Functionalized with Pralidoxime As a Material for Chemical Protection against Organophosphorous Compounds, ACS Applied Materials & Interfaces, (05 2011): 1479. doi: 10.1021/am200041e
07/09/2013	17.00	Lev Bromberg, Yaroslav Klichko, Emily P. Chang, Scott Speakman, Christine M. Straut, Eugene Wilusz , T. Alan Hatton. Alkylaminopyridine-modified aluminum amino terephthalate metal-organic frameworks as components of reactive self-detoxifying materials, ACS Applied Materials and Interfaces, (08 2012): 4595. doi:
08/10/2010	16.00	Lev Bromberg, Emily P. Chang, Carmen Alvarez-Lorenzo, Beatriz Magarinos, Angel Concheiro, and T. Alan Hatton. Binding of Functionalized Paramagnetic Nanoparticles to Bacterial Lipopolysaccharides And DNA, Langmuir, (01 2010): . doi:
12/01/2009	13.00	Lev Bromberg, Liang Chen, Emily P. Chang, T. Alan Hatton. DEGRADATION OF ORGANOPHOSPHATES BY SILVER AND COBALT NANOPARTICLES FUNCTIONALIZED WITH IMIDAZOLE LIGANDS, , (12 2009): . doi:

<b>TOTAL:</b>	<b>6</b>
---------------	----------

**Number of Papers published in peer-reviewed journals:**

---

**(b) Papers published in non-peer-reviewed journals (N/A for none)**

<u>Received</u>	<u>Paper</u>
-----------------	--------------

03/17/2009	7.00	Lev Bromberg, T. Alan Hatton. Poly(N-vinylguanidine): Characterization, and catalytic and bactericidal properties, Polymer, (11 2007): . doi:
03/17/2009	8.00	Lev Bromberg, T. Alan Hatton. Nerve Agent Destruction by Recyclable Catalytic Magnetic Nanoparticles, Industrial and Engineering Chemistry, Research, (09 2005): . doi:
03/17/2009	9.00	Lev Bromberg, T. Alan Hatton. Decomposition of Toxic Environmental Contaminants by Recyclable Catalytic, Superparamagnetic Nanoparticles, Industrial & Engineering Chemistry Research, (03 2009): . doi:

**TOTAL: 3**

**Number of Papers published in non peer-reviewed journals:**

---

**(c) Presentations**

**Number of Presentations: 0.00**

---

**Non Peer-Reviewed Conference Proceeding publications (other than abstracts):**

<u>Received</u>	<u>Paper</u>
-----------------	--------------

**TOTAL:**

**Number of Non Peer-Reviewed Conference Proceeding publications (other than abstracts):**

---

**Peer-Reviewed Conference Proceeding publications (other than abstracts):**

<u>Received</u>	<u>Paper</u>
-----------------	--------------

**TOTAL:**

**(d) Manuscripts**

<u>Received</u>	<u>Paper</u>
03/16/2009	2.00 Lev Bromberg, Svetlana Raduyk, T. Alan Hatton. FUNCTIONAL MAGNETIC NANOPARTICLES FOR BIODEFENSE AND BIOLOGICAL THREAT MONITORING AND SURVEILLANCE, Analytical Chemistry (02 2009)
03/17/2009	4.00 Lev Bromberg, T. Alan Hatton, Dan Carney, Heidi Schreuder-Gibson, William R. Creasy, David McGarvey, and Roderick A. Fry. DEGRADATION OF NERVE AGENTS BY POLYACRYLAMIDOXIME AND POLYESTER FABRIC TREATED BY POLYACRYLAMIDOXIME AS A REACTIVE BARRIER, (03 2009)
03/17/2009	6.00 Lev Bromberg, Huan Zhang, and T. Alan Hatton. Functional Organic–Inorganic Colloids Modified by Iodoxybenzoic Acid, Chemistry of Materials (01 2008)
05/27/2009	11.00 Lev Bromberg, Svetlana Raduyk, T. Alan Hatton. FUNCTIONAL MAGNETIC NANOPARTICLES FOR BIODEFENSE AND BIOLOGICAL THREAT MONITORING AND SURVEILLANCE, Analytical Chemistry (05 2009)
12/10/2009	15.00 L. Bromberg, E. P. Chang, C. Alvarez-Lorenzo, B. Magariños, A. Concheiro, T. A. Hatton. BINDING OF FUNCTIONALIZED PARAMAGNETIC NANOPARTICLES TO BACTERIAL LIPOPOLYSACCHARIDES AND DNA, (12 2009)
12/10/2009	14.00 L. Chen, L. Bromberg, J. A. Lee, a H. Zhang, H. Schreuder-Gibson, P. Gibson, J. Walker, P. T. Hammond, T. A. Hatton, G. C. Rutledge. MULTIFUNCTIONAL ELECTROSPUN FABRICS VIA LAYER-BY-LAYER ELECTROSTATIC ASSEMBLY FOR CHEMICAL AND BIOLOGICAL PROTECTION, Chemistry of Materials (09 2009)
<b>TOTAL:</b>	<b>6</b>

Number of Manuscripts:

---

**Books**

<u>Received</u>	<u>Paper</u>
-----------------	--------------

**TOTAL:**

**Patents Submitted**

L. Bromberg, T.A. Hatton, Catalytic nanoparticles for nerve-agent destruction, US Patent 7,598,199, October 6, 2009

~~T.A. Hatton, L. Bromberg, H. Zhang, Compositions for chemical and biological defense, and methods related thereto,~~  
Int.Pat.Appl., Pub. No.WO/2009/055128, Publication Date: 30.04.2009

L. Chen, L. Bromberg, T.A. Hatton, G.C. Rutledge, Bactericidal nanofibers, and methods related thereof, Pub. No.  
WO/2009/064767, Publication Date:22.05.2009.

### Patents Awarded

L. Bromberg, T.A. Hatton, Catalytic nanoparticles for nerve-agent destruction, US Patent 7,598,199, October 6, 2009

### Awards

#### Graduate Students

<u>NAME</u>	<u>PERCENT SUPPORTED</u>	Discipline
Liang Chen	0.33	
Emily Chang	0.33	
<b>FTE Equivalent:</b>	<b>0.66</b>	
<b>Total Number:</b>	<b>2</b>	

#### Names of Post Doctorates

<u>NAME</u>	<u>PERCENT SUPPORTED</u>
Sa Wang	1.00
<b>FTE Equivalent:</b>	<b>1.00</b>
<b>Total Number:</b>	<b>1</b>

#### Names of Faculty Supported

<u>NAME</u>	<u>PERCENT SUPPORTED</u>
<b>FTE Equivalent:</b>	
<b>Total Number:</b>	

#### Names of Under Graduate students supported

<u>NAME</u>	<u>PERCENT SUPPORTED</u>
<b>FTE Equivalent:</b>	
<b>Total Number:</b>	

### Student Metrics

This section only applies to graduating undergraduates supported by this agreement in this reporting period

The number of undergraduates funded by this agreement who graduated during this period: ..... 0.00

The number of undergraduates funded by this agreement who graduated during this period with a degree in science, mathematics, engineering, or technology fields:..... 0.00

The number of undergraduates funded by your agreement who graduated during this period and will continue to pursue a graduate or Ph.D. degree in science, mathematics, engineering, or technology fields:..... 0.00

Number of graduating undergraduates who achieved a 3.5 GPA to 4.0 (4.0 max scale):..... 0.00

Number of graduating undergraduates funded by a DoD funded Center of Excellence grant for Education, Research and Engineering:..... 0.00

The number of undergraduates funded by your agreement who graduated during this period and intend to work for the Department of Defense ..... 0.00

The number of undergraduates funded by your agreement who graduated during this period and will receive scholarships or fellowships for further studies in science, mathematics, engineering or technology fields: ..... 0.00

### Names of Personnel receiving masters degrees

NAME

**Total Number:**

### Names of personnel receiving PHDs

NAME

Liang Chen

Emily Chang

**Total Number:**

2

### Names of other research staff

NAME

Lev Bromberg

**FTE Equivalent:**

**Total Number:**

PERCENT SUPPORTED

0.25

**0.25**

**1**

### Sub Contractors (DD882)

### Inventions (DD882)

**5 Catalytic nanoparticles for nerve-agent destruction**

Patent Filed in US? (5d-1) Y

Patent Filed in Foreign Countries? (5d-2) N

Was the assignment forwarded to the contracting officer? (5e) Y

Foreign Countries of application (5g-2):

5a: Lev Bromberg

5f-1a: Massachusetts Institute of Technology

5f-c: 77 Massachusetts Avenue

Cambridge MA 02139

5a: T. Alan Hatton

5f-1a: Massachusetts Institute of Technology

5f-c: 77 Massachusetts Avenue

Cambridge MA 02139

**Scientific Progress**



## ABSTRACT (Maximum 13 lines, use the attachment if necessary)

Specific aims included studies of catalytic nanoparticles modified with nucleophilic ligands that can self-assemble and bind the metal (Ag, Co) particles cores as well as cationic and membrane-binding organic ligands and polymers and methodologies of surface modification with bactericidal species. We concentrated on the mechanisms of binding of the bactericidal nanoparticles to Gram-negative microorganisms.

Mechanistic studies of esterolytic reactions with paramagnetic nanoparticles.

Novel nucleophilic ligands were synthesized from oleic acid conjugated with 2-mercaptoimidazole via a UV-initiated thiol-ene reaction, and by a condensation of trans-9,10-epoxystearic acid with 4(5)-imidazoledithiocarboxylic acid. Nanoparticles (NPs) with 10-100 nm Ag(0) or Co(0) cores were obtained by reduction of Ag<sup>+</sup> or Co<sup>2+</sup> by borohydride in N,N-dimethylformamide or aqueous solutions, respectively. The NPs capped with oleic acid or 9,10-epoxystearic acids were further covalently bound to 2-mercaptoimidazole or 4(5)-imidazoledithiocarboxylic acid. The ligands and NPs functionalized with nucleophilic imidazole moieties enabled facile hydrolysis of paraoxon (O,O-diethyl O-(p-nitrophenyl) phosphate) by NPs in their aqueous media. The NPs acted as recoverable semi-heterogeneous catalysts. The paraoxon hydrolysis was accelerated 10- to 50-fold by the formation of complexes between the imidazole-containing ligands or NPs with Co<sup>2+</sup>.

Protective, bioactive nanoparticles. Magnetite and metallic cobalt-based nanoparticles with sizes ranging from 10 to 300 nm and surface-functionalized with poly(hexamethylene biguanide) (PHMBG) were discovered as capable lipopolysaccharide (LPS)-sequestering agents. The nanoparticles efficiently bind to whole E.coli cells and can be used to separate the cells effectively from suspension using a magnet. A fluorescence dye displacement assay shows strong affinities of the nanoparticles for lipid A, the glycolipid component of LPS responsible for septic shock. The particle-lipid A affinity is of the same order of magnitude or higher than that of polymyxin B. The affinity of smaller (<50 nm) magnetite particles modified with PHMBG to lipid A is several-fold higher than that of their larger counterparts (>100 nm) due to their higher surface area to volume ratio. The nanoparticles possess high saturation capacity for double-stranded DNA from E.coli, with which particle-polyelectrolyte complexes are formed. The PHMBG-modified nanoparticles are potent bactericides, inhibiting E.coli viability and growth at concentrations  $\leq 10$   $\mu$ g/mL.

## SCIENTIFIC PROGRESS AND ACCOMPLISHMENTS

Mechanistic studies of esterolytic reactions with paramagnetic nanoparticles

Transition metal and metal oxide nanoparticles have generated significant interest due to their large surface-to-volume ratios, functional properties and important applications, ranging from electronics and catalysis to biomedicine. In the reporting period, our specific area of interest has been nanoparticles (NPs) with a metal or metal oxide core that is functionalized with an organic ligand, either a small molecular weight species or a polymer, tailored for the destruction of toxins. Our NP design is based on the reactivity of the ligand, and not on the catalytic properties of a transition metal per se. The core of the ligand-decorated NP is non-reactive, but determines the NP shape and size, while facilitating the particle recoverability. The NPs can be readily recovered from the reaction medium by centrifugation or filtration. Large surface area, small thickness (up to 10% of the total hydrodynamic diameter of a given NP) and compatibility of the ligand shell with the continuous phases ensure accessibility of the reactive ligands to the reagents.

Our catalytic NP is a hybrid between the supported transition metal particles and functional polymeric colloids. Because of the multifunctionality of the organic ligands, our NPs are not only capable of carrying out catalytic functions, but can also bind strongly to bacterial membranes and kill various germs, thus acting as efficient disinfectants. In the previous reports, the majority of the ligands we employed to impart esterolytic function to the NP and other colloids have been oximes, hydroxamic acids, iodosobenzoates and other  $\pi$ -nucleophiles. While capable of facile hydrolysis of organophosphorous (OP) pesticides and chemical warfare agents,  $\pi$ -nucleophiles are quite sensitive to the presence of compounds that are not targeted and can also undergo transformations rendering them unreactive, such as Beckmann and Lossen rearrangements. Therefore, in the present work our goal was to create NPs functionalized with imidazole derivatives.

Polymers and nanosized assemblies functionalized with imidazole catalyze esterolytic and proteolytic reactions. The mechanism of the ester hydrolysis catalysis by low molecular weight imidazole derivatives is a function of the ester (substrate) structure. Esters that possess poor leaving groups are subject to classical general base catalysis by imidazole, while esters with good leaving groups are subject to nucleophilic catalysis. In polymers and colloidal assemblies, the activity of the imidazole group (much like in enzymes), depends on its microenvironment such as the presence of hydrophobic or hydrophilic moieties, as well as other imidazole groups, in its proximity. In that regard, we were interested in potential neighboring effects of the imidazole groups concentrated in the organic shell, on esterolytic reactions. It has been shown that self-assembling monolayers of various ligands form a multitude of patterns on the NP surfaces, which affect the microenvironment of the ligands and hence the NP solvation and its interaction with substrates. The confinement of the catalytic units to the monolayer covering the NP triggers a cooperative, pH-dependent hydrolytic mechanism in which an imidazolium ion acts as a catalyst. In the reporting period, we created functional fatty acid-imidazole conjugates for the NP surface modification. Because oleic acid is strongly surface-active and possesses a reactive unsaturated bond, we concentrated on its use for conjugating with imidazole derivatives, along with its epoxidized derivative, trans-9,10-epoxystearic acid. Thiol-ene coupling reactions involving the double bond of oleic acid and its esters are known. Commercially available derivatives of imidazole such as 2-mercaptoimidazole and 4(5)-imidazoledithiocarboxylic acid were chosen for conjugation with oleic acid and its derivative. 2-Mercaptoimidazole is a reactive, neutral nucleophile (pKa of the thiol group ionization, 11.6) capable of participating in thiol-ene reactions, which are

facilitated by the relatively low S-H bond dissociation energy, and even more readily, in conjugation reactions with epoxy groups. 2-Mercaptoimidazole is also a bioactive metal-complexing agent. Testing of the hydrolytic activity of the ligands and nanoparticles was performed using the insecticide paraoxon as a substrate. Hydrolysis of paraoxon and analogous OP pesticides catalyzed by metal ions, micelles of nucleophilic surfactants and metallomicelles and enzymes has been studied in detail and such hydrolysis represents a convenient reaction reflecting upon the activity of the catalytic agent used. Although the hydrolysis of paraoxon is of practical importance in its own right from an environmental standpoint, it can also serve as a mechanistic model of degradation of more toxic warfare agents. We chose cobalt and silver to be the cores of our NPs, as their synthesis and detection are well-established, yet fatty acids are capable of binding through their carboxylic groups with the surfaces of these metals. Based on the above-described rationale, in the present work we designed and synthesized water-dispersible NPs with silver or cobalt cores functionalized by shells of fatty acids modified with imidazole derivatives. The NPs are reactive toward paraoxon, especially in the presence of cobalt (II) ions.

Syntheses were accomplished as follows.

Conjugate of oleic acid and 2-mercaptoimidazole (10-((1H-imidazol-2-yl)thio)octadecanoic acid) (1) (Fig. 1)

A solution of oleic acid (1.0 g, 3.54 mmol), 2-mercaptoimidazole (0.354 g, 3.54 mmol), and benzophenone (50 mg, 0.27 mmol) in 10 mL dry methanol was deaerated and placed in a glass vial, which was subsequently sealed and irradiated using a UV-Vis 5000EC flood lamp (spectral output, 300-500 nm; maximum intensity, 250 mW/cm<sup>2</sup> at 365 nm; Dymax Corp, Torrington, CT) for 10 min. The resulting yellow solution was equilibrated at ambient temperature and vacuum-evaporated. The products were separated by TLC (silica gel, aluminum oxide sheets Si 60 F254, 5x10 cm, EMD Chemicals, Gibbstown, NJ) using hexane-ethyl acetate (80:20 v/v). Yield, 75%. The initial compounds moved with the solvent front; the product observed under UV ( $R_f$  0.5) was separated and dissolved in 250  $\mu$ L of CD<sub>3</sub>OD. <sup>1</sup>H NMR (CD<sub>3</sub>OD, 400 MHz, Supporting Information, S1),  $\delta$  (ppm): 6.8 (2H, imidazole), 3.2 (1H, methine,  $\delta$  to C-S), 2.3 (2H, methylene,  $\delta$  to COOH), 1.55 (2H, methylene), 1.1-1.3 (22H, methylene), 0.87 (3H, methyl). Found (calc): C, 65.1 (64.82); H, 9.26 (10.34); N, 6.93 (7.56); S, 8.29 (8.65). Solubility compound (1) was tested at room temperature and at 2.5 mM concentration level. Compound (1) formed clear solutions in water at pH>5, methanol, ethanol, DMF and DMSO.

Fig.1.

Conjugate of trans-9,10-epoxystearic and imidazoledithiocarboxylic acids ((9S,10S)-1,1,10-trihydroxyoctadecan-9-yl 1H-imidazole-5-carbodithioate) (2) (Fig. 2)

trans-9,10-Epoxystearic acid (30 mg, 0.1 mmol) and 4(5)-imidazoledithiocarboxylic acid (15 mg, 0.1 mmol) were dissolved in 1 mL of N,N-dimethylformamide and the reaction was conducted in a sealed vial at 70°C for 24 h. The initial reaction solution was dark-red and became brown at the end of the reaction. The products were purified as follows. The reaction mixture was allowed to cool to ambient temperature and excess deionized water (15 mL) was added. Dark-brown precipitates formed. The precipitates were centrifuged (12,900 g, 15 min) and separated. The solids were redissolved in cold acetone (4°C, 15 mL). Upon heating to 70°C, dark-red precipitates were formed in the acetone. The solids were separated from the hot acetone by centrifugation and residual solvent was evaporated under vacuum. Yield, 83%. The TLC in ethanol/acetone (1:1) mixture showed one product ( $R_f$  0.5). <sup>1</sup>H NMR (DMF-d<sub>7</sub>, 400 MHz, S2),  $\delta$  (ppm): 12.9 (1H, imidazole), 12.1 (1H, H-O-C(=O)), 7.88 (1H, imidazole), 3.48 (1H, methane), 2.24, 151 (2H, methylene), 1.25-1.44 (24H, methylene), 0.88 (3H, methyl). Found (calc): C, 60.1 (59.69); H, 8.59 (8.65); N, 6.05 (6.33); S, 13.9 (14.49). Compound (2) was water-soluble at pH>8.5 and dissolved in acetone, DMF-d<sub>7</sub> and DMSO at 2.5 mM and room temperature.

Fig. 2.

Synthesis of Co(0) nanoparticles without capping agents

Cobalt chloride hexahydrate (238 mg, 1.0 mmol) dissolved in 15 mL ethylene glycol was mixed with an aqueous solution of NaOH (2 mmol in 20 mL). Hydrazine (1.6 g, 50 mmol) was slowly added to the resulting solution via syringe and the mixture was briefly sonicated and kept at 80°C for 5 h, with intermittent vortexing. The formed particles were then separated from the supernatant by centrifugation (12,900 g, 5 min) and washed with excess ethanol, followed by centrifugation and repeated washing. The wash-outs were diluted 3-fold by deionized water and the pH of the resulting solution was measured to be 7.6, indicating that the excess hydrazine and sodium hydroxide was removed. The resulting particles were separated by centrifugation, dried under vacuum and stored in a desiccator in oxygen-free conditions, to prevent cobalt oxidation. For DLS measurements, the particles were dispersed in deionized water by brief sonication and then the number-average hydrodynamic diameter of the particles was measured within 1-2 min to be 7.1 $\pm$ 1.3 nm.

Synthesis of Co(0) nanoparticles modified by 9,10-trans-epoxystearic acid

Cobalt nanoparticles prepared without capping agents (20 mg) were suspended in a solution of 9,10-trans-epoxystearic acid (30 mg, 0.1 mmol, dissolved in 1.0 mL methanol) and briefly sonicated. To the suspension, 5 mL of deionized water was added and the suspension was vortexed. The particles were then separated from the reaction mixture by centrifugation at 12,900 g, suspended in 20 mL deionized water with brief sonication and the procedure of washing and separation was repeated three times. The resulting Co(0) particles were water- and organic solvent-dispersible. The particles were characterized by DLS in water (pH 7), thermogravimetric analysis and SQUID. The particles were found to have a number-average hydrodynamic diameter of 26 $\pm$ 11 nm, a saturation magnetization of ~ 25 emu/g of cobalt and a fatty acid content of 22 wt%.

Synthesis of Co(0) nanoparticles modified by oleic acid

A solution of oleic acid (30 mg, 106  $\mu$ mol, dissolved in 1.0 mL methanol) was suspended in 8 mL deionized water using brief sonication. To the suspension, a solution of cobalt chloride hexahydrate (238 mg, 1.0 mmol, dissolved in 2 mL water) was

added, resulting in a pink-colored, opaque suspension, to which a solution of sodium borohydride (100 mg, 2.6 mmol in 3 mL water) was added under stirring. Foaming and formation of black-colored particles was observed. The reaction was allowed to proceed in a sealed flask for 16 h at room temperature with shaking. In a separate set of experiments, a freshly prepared solution of 2-mercaptoimidazole (150 mg, 1.5 mmol in 10 mL water) was added first followed by addition of sodium borohydride (100 mg, 2.6 mmol in 3 mL water) to cobalt chloride hexahydrate and oleic acid suspension as above. The reaction was allowed to proceed identically to the one without 2-mercaptoimidazole. The particles were separated from the reaction mixture by centrifugation at 12,900 g and suspended in 50 mL deionized water with brief sonication and the procedure of washing and separation was repeated three times. The resulting Co(0) particles were characterized by TEM, DLS in water (pH 7), thermogravimetric analysis and SQUID. After washing, the Co and S composition (wt%) of the cubical cobalt nanoparticles was: Co, 83.0; S, 0.75. No sulfur was detected in the particles prepared without 2-mercaptoimidazole. SQUID analysis of the cobalt NP modified with oleic acid yielded a saturation magnetization of approximately 25 emu/g of cobalt.

#### Synthesis of silver nanoparticles in DMF

Silver nanoparticles were prepared by the reduction of AgNO<sub>3</sub> in N,N-dimethylformamide (DMF). In a typical experiment, silver nitrate (2 g) and sodium borohydride (200 mg) were dissolved separately, each in 25 mL of DMF. Then, the borohydride solution was added dropwise into the silver nitrate solution in DMF. The color of the solution became black. The suspension was stirred and kept at 80°C for 1 h to complete the reaction. At the end, a black precipitate was formed, which was centrifuged at 12,900 g and purified by washing with acetone, which was repeated 3 times to remove the excess DMF. The black precipitate was dried in a vacuum oven at 50 °C.

#### Synthesis of silver nanoparticles modified by oleic or 9,10-trans-epoxystearic acid

The black powder of silver particles prepared in DMF was dispersed in 15 mL of oleic acid (initial particle amount, 220 mg) or a solution of 9,10-trans-epoxystearic acid (50 mg acid 1 mL of DMF; initial particle amount, 30 mg), which was vortexed and vigorously shaken for 24 h at room temperature. The capped silver nanoparticles were centrifuged at 12,900 g and purified by washing with absolute ethanol. This process was repeated three times in order to remove the excess capping acid. Further removal of ethanol by vaporizing and drying in a vacuum oven gave a bright-black, dry powder of surface-modified silver nanoparticles. The particles capped with oleic and epoxystearic acid contained 24 and 16 wt% of corresponding fatty acids, respectively.

#### Synthesis of Ag and Co nanoparticles modified by 2-mercaptoimidazole and oleic acid conjugate (1)

The oleic acid-capped Ag or Co particles (Co particles were prepared with the use of 2-mercaptoimidazole) were further modified by conjugating 2-mercaptoimidazole with oleic acid on the particle surface using the thiol-ene reaction. Namely, 25 mg of particles modified with oleic acid were suspended in 2 mL of dry methanol with brief sonication, a solution of 2-mercaptoimidazole (4 mg, 40  $\mu$ mol) and benzophenone (2 mg, 11  $\mu$ mol) in 2 mL dry methanol was added, and the mixture was deaerated and placed in a glass vial, which was subsequently sealed and irradiated using a UV-Vis 5000EC flood lamp (spectral output, 300-500 nm; maximum intensity, 250 mW/cm<sup>2</sup> at 365 nm; Dymax Corp, Torrington, CT) for 10 min. The resulting opaque suspension was equilibrated at ambient temperature, vacuum-evaporated, and resuspended in methanol (20 mL), following which the particles were separated by centrifugation (12,900 g, 5 min). The procedure of washing with methanol was repeated three times and the particles were vacuum-dried and kept at 40°C prior to the use. The particles were visualized by TEM. Silver particles modified with conjugate (1) (designated Silver NP-(1)) appeared to be aggregates of spherical particles of ~10 nm diameter, with the aggregate size of approximately 200 nm (S4), whereas modified Co particles (designated Cobalt NP-(1)) were cubical or octahedral, with an average size of ~100 nm (S5). These observations were corroborated by DLS measurements in water (pH adjusted to 7), yielding number-average hydrodynamic diameters of 190 and 130 nm for Silver NP-(1) and Cobalt NP-(1), respectively. TGA yielded the contents of Ag and Co to be 77 and 80 wt% in Silver NP-(1) and Cobalt NP-(1), respectively. SQUID measurements yielded a saturation magnetization of Cobalt NP-(1) to be 6.7 emu/g of cobalt. Elemental analysis found, for Silver NP-(1): C, 15.2; H, 2.51; Ag, 76.9; N, 1.68; S, 1.04; and found, for Cobalt NP-(1): C, 13.4; H, 2.31; Co, 77.4; N, 2.44; S, 2.95.

#### Modification of Ag or Co nanoparticles with epoxystearic and 4(5)-imidazoledithiocarboxylic acids conjugate (2)

The silver or cobalt NPs capped with 9,10-trans-epoxystearic acid (25 mg) were suspended in a solution of 4(5)-imidazoledithiocarboxylic acid (14 mg, 0.1 mmol, dissolved in 1.0 mL DMF) and the resulting suspension was kept at 70°C for 8 h with intermittent vortexing. The resulting particles were separated by centrifugation (12,900 g, 5 min), diluted with 20 mL ethanol, briefly sonicated, and again separated by centrifugation. The procedure was repeated three times. The resulting particles were dried under vacuum and characterized by TGA, TEM, (S6) and elemental analysis. SQUID measurements yielded a saturation magnetization of Cobalt NP-(2) to be approximately 2.0 emu/g of cobalt (S3). TGA measured the contents of Ag and Co to be 82 and 79 wt% in Silver NP-(2) and Cobalt NP-(2), respectively. Elemental analysis found, for Silver NP-(2): C, 11.8; H, 1.58; Ag, 81.0; N, 1.18; S, 2.69; and found, for Cobalt NP-(2): C, 13.1; H, 1.91; Co, 78.7; N, 1.43; S, 3.11.

#### Complexes of ligands and nanoparticles with Co<sup>2+</sup>

Complexes of ligands and nanoparticles with Co<sup>2+</sup> were prepared by suspending the corresponding species in deionized water at 3-4 mg/mL concentration and adding an aqueous solution of cobalt(II) chloride hexahydrate (5 mL) resulting in a cobalt concentration that was equimolar to the corresponding ligand. The resulting suspension was separated by centrifugation (12,900 g, 20 min) and the remaining blue paste or solids were lyophilized and stored at -20°C prior to the use.

#### Characterization by NMR

NMR spectroscopy and kinetics of paraoxon hydrolysis. <sup>1</sup>H and <sup>31</sup>P NMR spectra were collected at 25±0.5 °C using a Bruker Avance-400 spectrometer operating at 400.01 and 161.98 MHz, respectively. <sup>1</sup>H NMR spectra were measured with solutions of

ligands in deuterated solvents. The kinetics of paraoxon degradation were determined using  $^{31}\text{P}$  NMR. Spectra (1500 scans for cobalt chloride solutions and 64 scans for all other samples) were recorded using an 85% phosphoric acid solution in  $\text{D}_2\text{O}$  as an external reference (0 ppm). The reaction milieu consisted of 50 mM HEPES buffer in  $\text{D}_2\text{O}$  to keep the solution pH constant at 9. The reaction time was taken to be the midpoint of the acquisition period. For kinetic measurements with non-magnetic materials, samples of 2-3 mg/mL of ligand or silver nanoparticle-based suspension in HEPES/ $\text{D}_2\text{O}$  solution (50 mM, pH 9.0) and paraoxon solution in acetonitrile (50 mM) were prepared. Basic pH accelerated the spontaneous hydrolysis of paraoxon to acceptable levels versus neutral pH, and buffering allowed for maintenance of constant reaction rate up to high degrees of conversion. Acetonitrile was added to improve the miscibility of paraoxon (aqueous solubility at  $20^\circ\text{C}$ , up to 3.6 mg/mL) and aqueous buffer as well as to act as a convenient reactant diluent that did not trigger the reaction prior to contact with the aqueous phase. At  $t=0$ , 630  $\mu\text{L}$  of ligand or non-magnetic particle suspension and 70  $\mu\text{L}$  of paraoxon solution were mixed by vortexing and placed into an NMR tube for kinetic measurements. Paramagnetic cobalt NP-based suspensions (3 mg/mL) in HEPES/ $\text{D}_2\text{O}$  buffer (50 mM, pH 9.0) were prepared as a 5-mL stock sample, which was mixed with 556  $\mu\text{L}$  of paraoxon in acetonitrile at  $t=0$ , resulting in the initial paraoxon concentration of 5 mM. The final suspension was kept at room temperature while shaking. At given time intervals, the suspension was centrifuged (6,500 g, 5 min), and the top clear solution (0.7 mL) was carefully withdrawn by a pipette and placed into an NMR tube. The solution was placed back into the suspension immediately after each NMR measurement. The degree of paraoxon conversion was expressed as:

$$F_t = \Sigma I_p / (\Sigma I_r + \Sigma I_p), \quad (1)$$

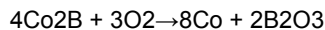
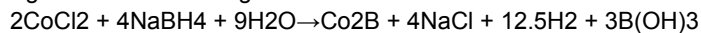
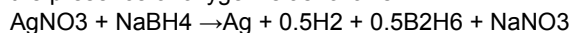
where  $\Sigma I_r$  and  $\Sigma I_p$  are the sums of the integrations of the signals corresponding to the reactant (paraoxon, -6.11 ppm) and the products (diethyl phosphate, 1.22 ppm, and diethyl phosphate-HEPES adduct), respectively (S7). The observed rate constant,  $k_{\text{obs}}$ , is found from the slope of the  $\ln(1 - F_t)$  vs.  $t$  plot:

$$\ln(1 - F_t) = -k_{\text{obs}} t \quad (2)$$

Ligand and particle syntheses and characterization

In the reporting period, we wished to develop a straightforward synthetic route toward fatty acids that are modified by a reactive moiety capable of chelating with transition metal ions and accelerating the hydrolysis of organophosphorous esters. Neither 9-((1H-imidazol-2-yl)thio)octadecanoic acid (1) nor 9-((1H-imidazole-5-carbonothioyl)thio)-8-hydroxyoctadecanoic acid (2) and their syntheses via the thiol-ene reaction of oleic acid and 2-mercaptoimidazole (Fig. 1), and trans-9,10-epoxystearic and 4(5)-imidazoledithiocarboxylic acids (Fig. 2), respectively, have been previously reported. The one-step synthetic routes described herein are facile and produce acceptable yields, limited only by the product purification processes, as is common for fine fatty acid derivatives. The targeted fatty acid derivatives (1) and (2) are multidentate ligands with thiol, amine, and carboxylic groups capable of complexation with metal ions. Thiol sulfur, dithiocarboxylic moieties and imidazole nitrogens possess inherently stronger coordination and chelation capability with metals than do carboxyl groups. Therefore, in order to maintain the NP complexation by fatty acids through metal-carboxyl binding, we synthesized oleic acid- or epoxystearic acid-modified particles, which were subsequently modified by 2-mercaptoimidazole or (4)5-imidazoledithiocarboxylic acid. If we were to bind multidentate compounds (1) and (2) to cobalt or silver NP directly, the metal-thiol or metal-imidazole chelation would have been more likely than metal-carboxyl.

Notably, in our synthetic route, the nanoparticles were first prepared by reduction of the corresponding cobalt or silver salts by sodium borohydride, purified and then complexed with fatty acids. Reduction of silver and cobalt salts by sodium borohydride in the presence of oxygen is as follows:



In the case of  $\text{Co}(\text{II})$ , when the mixture is exposed to oxygen, a sacrificial reaction takes place whereby boron is oxidized while cobalt is reduced, resulting in the conversion of  $\text{Co}_2\text{B}$  to  $\text{Co}(\text{metal})$ .

Interestingly, the structures of the Co NPs prepared with and without 2-mercaptoimidazole appeared to be quite different.

Particles prepared with oleic acid as the only capping agent aggregated into  $\sim 200$  nm clusters composed of  $\sim 10$  nm spherical primary particles, whereas the particles prepared in the presence of both 2-mercaptoimidazole and oleic acid were cubical or octahedral in shape, with one side of the cube sized  $\sim 50$  nm. Although the formation of cubical particles in the presence of both mercaptoimidazole and oleic acid is a novel observation of the present study, it has been reported previously that simultaneous presence of several agents strongly binding to the nanocrystal surface such as oleic acid, trioctylphosphine oxide and others affects the shape of the cobalt crystals.

The reduction of silver sulfate by borohydride directly in the presence of oleic acid could result in the binding of the silver nanoparticle surface to the oleic acid through the double bond. In our synthesis, because the reduction was completed prior to the contact of fatty acids with the resulting NP, the adsorption of the fatty acids on the Ag or Co surface is through the carboxylate groups. The  $\zeta$ -potential measured in 5 mM KCl at pH 7.0 was  $-22 \pm 3$  mV (silver-epoxystearic acid NP) and  $-28 \pm 2$  mV (cobalt-oleic acid NP), indicating that the particles are stabilized by the negative charge of the carboxylate groups exposed to the outer layer of the water-bilayer interface.

Modification of particles capped by oleic or epoxystearic acid by the thiol-ene reaction with mercaptoimidazole or condensation with imidazoledithiocarboxylic acid, respectively, was evident from FTIR data. Thus, FTIR spectra of the silver and cobalt NP-(1) and NP-(2) featured two strong bands at about 2920 and 2850  $\text{cm}^{-1}$ , typical of the antisymmetric and symmetric CH stretching vibrations, respectively, due to the fatty acid components. The spectra also showed bands characteristic of vibrations of the imidazole ring (amidine bands around 1640-1650  $\text{cm}^{-1}$ ), and C-C-S stretching bands at 686  $\text{cm}^{-1}$  (cobalt NP-(1)). The

strong band characteristic of the free carboxylate group at 1710 cm<sup>-1</sup> in the fatty acid as well as free conjugates (1) and (2) (not shown) was present only as a shoulder of a broader signal centered in the 1640 cm<sup>-1</sup> area in the NP spectra. Overall, the FTIR spectra support the structure wherein imidazole-containing conjugates are adsorbed onto the NP metal surfaces via carboxylate-metal complexation.

Further quantitative information on the ratio of metal to organic ligands comes from the TGA and elemental analysis (see Experimental section). Based on these analyses, we estimate that the average NP modified with conjugate (1) contained approximately one molecule of (1) per 25 silver and 27 cobalt atoms, respectively, whereas NP modified with conjugate (2) contained approximately one molecule of (2) per 18 silver and 27 cobalt atoms, respectively. Based on the elemental analysis, and assuming the average diameter of a single particle to be 10 nm, we estimate that the area occupied by a single ligand on Ag and Co nanoparticle surface in our experiments is in the range 0.08-0.15 nm<sup>2</sup>. For comparison, the mean molecular area occupied by a single oleic acid molecule is about 0.42 nm<sup>2</sup>/molecule. Given that the ligands (1) and (2) are significantly larger than the oleic acid molecule due to the attachment of the imidazole moieties, we can conclude that the ligands were attached to the NPs in multilayers.

#### Ligand and nanoparticle performance in organophosphate hydrolysis

We studied the performance of the ligands attached to the nanoparticles in the hydrolysis of the organophosphate insecticide, paraoxon. The kinetics of the insecticide hydrolysis was studied in aqueous solutions containing 10% acetonitrile. The pH was kept constant at 9.0 throughout the study. The basic pH accelerated the spontaneous hydrolysis of paraoxon to acceptable levels versus neutral pH, and buffering allowed for maintenance of constant reaction rate up to high degrees of conversion. The reaction was followed by <sup>31</sup>P NMR. When the kinetics results were expressed in terms of eqn(2), the curve fits were linear (R<sup>2</sup>>0.98 in all cases), indicating a pseudo first-order reaction order. The observed rate constants afforded calculation of the reaction half-life ( $t_{1/2} = \ln(2)/k_{obs}$ ) and the apparent second-order rate constant  $k'' = k_{obs}/C_{cat}$ , where  $C_{cat}$  is the initial effective molar concentration of the catalytic groups. The results of all kinetic measurements are collected in Table 1.

Table 1. Half-life ( $t_{1/2}$ ) and apparent second-order rate constant ( $k''$ ) of paraoxon hydrolysis in the presence of ligands and nanoparticles of the present study at pH 9.0.

aSystem (M-1s-1)	Half-life, $t_{1/2}$ (days)	b Second-order rate constant, $k'' \times 10^4$
Spontaneous hydrolysis	>140	
2-Mercaptoimidazole	35 1.2	
Stoichiometric complex		
2-mercaptoimidazole/Co <sup>2+</sup>	2.6 16	
4(5)-Imidazoledithiocarboxylic acid	11 3.6	
Stoichiometric complex		
4(5)-imidazoledithiocarboxylic acid/Co <sup>2+</sup>	6.6 6.1	
Silver NP-(1)	20 4.9	
Silver NP-(2)	24 1.5	
Stoichiometric complex		
Silver NP-(1)/Co <sup>2+</sup>	1.9 53	
Co <sup>2+</sup>	21 0.30	
Cobalt NP-(1) <sup>c</sup>	5.8 2.1	
Cobalt NP-(2)	32 0.38	
Stoichiometric complex		
Cobalt NP-(2)/Co <sup>2+</sup>	2.3 18	

aEach system comprised 10 v% acetonitrile solution in 50 mM HEPES/D<sub>2</sub>O (pD 9.0)

bApparent second-order rate constants were calculated from  $k'' = r_0/C_s C_{cat}$ , where  $r_0 = k_{obs} C_s$  is the initial reaction rate,  $C_s$  and  $C_{cat}$  are initial effective concentrations of the substrate (paraoxon) and catalyst, respectively. The  $C_{cat}$  values were calculated as effective molar concentrations of the catalytic groups.

cSynthesized in the presence of 2-mercaptoimidazole and oleic acid (see Experimental section).

The weakly nucleophilic 2-mercaptoimidazole afforded only approximately 4-fold faster paraoxon degradation compared to the spontaneous hydrolysis, but 4(5)-imidazoledithiocarboxylic acid was approximately 12-fold more active because of its higher nucleophilicity. Cobalt chloride solution per se was not particularly reactive. However, stoichiometric complexation of either of 2-mercaptoimidazole or 4(5)-imidazoledithiocarboxylic acid with cobalt ions resulted in a significant, up to 13-fold acceleration of the paraoxon hydrolysis. The same synergistic effect of the presence of both imidazole-containing ligands and cobalt ions was observed with nanoparticles modified with conjugates (1) and (2), where ligand complexation with Co<sup>2+</sup> resulted in 10 to almost 50-fold hydrolysis acceleration. Mechanistically, such a phenomenon can be explained by the ability of the Co<sup>2+</sup> or Co<sup>2+</sup>-imidazole ligand to coordinate the oxonate oxygen, withdrawing electron density away from the phosphorus atom and generating a more reactive electrophile capable of efficient hydrolysis even by moderately nucleophilic ligands such as imidazole. Schematics of both imidazole ligand- and ligand-Co<sup>2+</sup> mechanisms of hydrolysis are shown below:

Similarly, acceleration of the paraoxon hydrolysis has been observed with vinylimidazole-containing polymers chelated

("molecularly imprinted") with  $\text{Co}^{2+}$ . An analogy between such an active imidazole- $\text{Co}^{2+}$  complex and the active site of phosphotriesterase with  $\text{Co}^{2+}$  ions coordinated to histidine can be suggested. To the best of our knowledge, ours is the first encounter of such a "biomimetic" catalytic activity of nanoparticles complexed with metal ions.

Summary: mechanistic studies of organophosphate degradation with nanoparticles

For the first time, we described a facile synthesis of imidazole-containing ligands that are conjugated to fatty acid chains via a thiol-ene reaction between oleic acid and 2-mercaptoimidazole and a condensation between (4)5-imidazoledithiocarboxylic and 9,10-epoxystearic acids. To obtain the ligands bound to the metal surface by the carboxyl groups, we first synthesized NPs of  $\text{Ag}(0)$  and  $\text{Co}(0)$  by conventional reduction of corresponding salts by sodium borohydride. Then the adsorbed oleic or 9,10-epoxystearic acids were further modified by 2-mercaptoimidazole and (4)5-imidazoledithiocarboxylic acid, respectively. As a variation of the "fatty acid adsorption first" synthesis, we were able to obtain  $\text{Co}(0)$ -based NPs by reduction of  $\text{Co}^{2+}$  in the presence of both the fatty acid and 2-mercaptoimidazole, which unexpectedly resulted in the NPs of cubical or octahedral shape, as opposed to spherical particles formed in the presence of oleic acid only. The thio- and dithio- imidazole ligands and NPs demonstrated significant, albeit moderate activity in catalyzing esterolysis of paraoxon, but their complexes with  $\text{Co}^{2+}$  were 10- to 50-fold more reactive. The uncovered synergistic effect of the  $\text{Co}^{2+}$  (but not  $\text{Co}(0)$  in the nanoparticle core) and imidazole derivatives mimics that of the metal-histidine moieties in the active site of enzymes in that the metal-ligand complex is far more nucleophilic than the ligand itself. The described NPs were readily recovered from the reaction medium by filtering or centrifugation and in that sense were advantageous as catalysts over their organic ligands without the metal core. In addition, the metal cores resulted in intense coloring of the particles, which can be exploited for particle detection.

Studies of interactions of paramagnetic nanoparticles with cell membranes

Endotoxins, or lipopolysaccharides (LPS), the prominent structural component of the outer membrane of Gram-negative bacteria, play a central role in septic shock, a syndrome of systemic toxicity that develops after serious Gram-negative infections, accounting for over 200,000 deaths in the US annually. The toxicity of LPS stems from its glycolipid component termed lipid A, which consists of a hydrophilic bis-phosphorylated glycosamine backbone and a hydrophobic cluster composed of acyl chains in amide and ester linkages. One of the approaches toward Gram-negative sepsis therapy is to target LPS by the use of binding and sequestering agents. Successful LPS sequestrants contain positively charged groups allowing for proper steric complementarity to the two anionic phosphates of lipid A, in order to form an ionic complex. The sequesterant affinity for lipid A can be further enhanced by pendant hydrophobic segments that stabilize the sequesterant-lipid A complex via hydrophobic interactions with the polyacyl domain of lipid A. A well-known, broad-range antiseptic, poly(hexamethylene biguanide) (PHMBG) possesses both biguanide groups that are sterically complementary to the LPS phosphate groups and hydrophobic hexamethylene segments. In the previous report, we proposed a concept for nanoparticle-based environmental monitoring, where magnetite nanoparticles functionalized with PHMBG are captured, together with germs bound to the particle surface, by a high gradient magnetic separation (HGMS) process, and the microorganism's DNA is extracted and analyzed by real-time polymerase chain reaction. The magnetite itself is not bactericidal. Importantly, the toxicity of such particles to mammalian cells appeared to be many-fold lower than that toward microorganisms. The particles enable not only in-situ biodefense, but also a method of monitoring aqueous habitats for the presence of dangerous germs. In the present study, the PHMBG-modified magnetic particles are viewed as a novel LPS sequesterant and their interactions with lipid A are quantified. Furthermore, since the particles can encounter and bind soluble DNA either in water or upon penetration to the cell interior, their binding capacities toward DNA are presented as well. For consistency, the source of both lipid A and DNA that were utilized in this study was *Escherichia coli*.

Experiments

Polyethyleneimine-modified magnetite (PEI-M). Magnetic nanoparticles were synthesized by chemical coprecipitation of iron (II) and iron (III) chlorides. Namely, 13.52 g (50 mmol) of  $\text{FeCl}_3 \cdot 6\text{H}_2\text{O}$  and 4.97 g (25 mmol) of  $\text{FeCl}_2 \cdot 4\text{H}_2\text{O}$  were added to 200 mL of deionized water and the solution was deaerated by nitrogen purge in a stirred 250-mL three-necked flask for 0.5 h. The temperature of the flask contents was then brought to 60°C. An aqueous solution containing PEI (5 g polymer in 40 mL water, pH adjusted to 6) and fluorosurfactant Zonyl 9373 (0.5 g)<sup>7</sup> was added to the flask and the resulting mixture was equilibrated at 80°C for 15 min while gently stirring under nitrogen purge. Then the nitrogen purge was ceased and the contents of the flask were at once added to 100 mL of a 28% ammonium hydroxide solution; the mixture, which rapidly turned black, was stirred vigorously for 5-10 min. The resulting precipitate was kept at 90°C for 1 h and separated from the liquid by decantation using a Franz Isodynamic Magnetic Separator (Trenton, NJ). The precipitate was resuspended in deionized water with sonication, dialyzed against excess DI water (membrane MW cut-off, 12-14 kDa) and lyophilized. Elemental analysis (%): C, 26.7; H, 5.53; Fe, 39.8; N, 12.4.

Poly(hexamethylene biguanide)- and polyethyleneimine-modified magnetite (PHMBG-PEI-M). PEI-M particles (2 g) were suspended in 20 mL of 5 wt% PHMBG aqueous solution with sonication for 30 s. To this suspension, 10 mL of 25% aqueous glutaraldehyde were added and the resulting suspension was quickly stirred and then shaken at room temperature for 16 h. The resulting suspension was dialyzed against excess DI water (membrane MW cut-off, 12-14 kDa) and lyophilized. The black solids were suspended at 1-2 wt% in deionized water using a Branson sonifier, resulting in polydisperse particle population designated PHMBG-PEI-M (t). The dispersion was fractionated using high-gradient magnetic separation (HGMS) as follows. Particle fractionation. The PHMBG-PEI-M particle dispersion was passed, by means of a hand-driven piston, through a

polypropylene syringe with an internal diameter of 5 mm and a length of 7 cm tightly packed (packing length, 30 mm) with 0.21 g of type 430 fine-grade stainless steel wool (40-66 mm diameter) supplied by S. G. Frantz Co., Inc. (Trenton, NJ) placed inside a Model L-1CN separator (Frantz Co.). The maximum flux density generated inside the magnet separator was 1.3 T. After the HGMS, the smaller particles were not captured and thus washed off; the wash-outs were collected and lyophilized, resulting in a fraction designated PHMBG-PEI-M (s). In order to remove the captured particles from the steel wire, the electromagnet was turned off and the particles no longer attracted to the wire by magnetic force were washed away by DI water passing through the wire column. The dispersion of particles captured by the wire column and washed by DI water was lyophilized resulting in a fraction designated PHMBG-PEI-M (l). Elemental analysis (%), PHMBG-PEI-M (t): C, 29.0; H, 6.04; Fe, 36.6; N, 14.3; PHMBG-PEI-M (s): C, 27.8; H, 5.86; Fe, 36.7; N, 14.0; PHMBG-PEI-M (l): C, 26.9; H, 7.15; Fe, 37.1; N, 14.2.

Copolymer of poly(hexamethylene biguanide) and polyethyleneimine (PHMBG-PEI; Mn, 1800 Da) was synthesized as described in detail in our previous publication. The copolymer (PEI:PHMBG, 1:1 w/w) mimicked the composition of the polymer formed on the surface of magnetite particles and was used as a positive control in the dye displacement measurements.

**Poly(hexamethylene biguanide)-Cobalt Particles.** To an aqueous solution containing 1.0 g (4.2 mmol) cobalt chloride hexahydrate and 0.8 g (0.5 mmol per number-average molecular weight) of PHMBG, a freshly prepared aqueous solution of 0.31 g (8 mmol) sodium borohydride (40 mL total) was added dropwise and the mixture was stirred for 1 h at room temperature. When the gas formed had largely evolved, the mixture was shaken in a sealed vial overnight and the solid, black precipitate was separated using centrifugation (5,000 g, 5 min), the pellet was resuspended and washed by water with sonication and then the solids were separated by magnetic decantation. The washing and separation procedure was repeated four times. The solids were then resuspended in water, dialyzed against excess DI water (membrane MW cut-off, 12-14 kDa) and lyophilized.

#### Fluorescence displacement assay

The dye displacement assay was performed as follows. To 3 mL of 5  $\mu$ M solution of BC in 50 mM Tris buffer, 2-5  $\mu$ L aliquots of either LPS or lipid A solution (1 mg/mL) in the same buffer were added and the mixture was sonicated for a few seconds, resulting in a transparent solution. The solution was placed in a cuvette and the steady-state fluorescence emission spectrum was measured in the 590-750 nm range (excitation, 580 nm). The addition of LPS or lipid A results in concentration-dependent quenching of BC without any changes in the emission peak maximum ( $\lambda_{\text{max}}$ =618 nm). After addition of aliquots of lipid A to the BC solution and measurements, the solutions were titrated with 2-20  $\mu$ L aliquots of 0.03-0.05 mg/mL suspensions of nanoparticles or solutions of either 2  $\mu$ M Polymyxin B (PMB, positive control) or 0.25 mM PHMBG in 50 mM Tris buffer. After each aliquot addition, the suspension was vortexed briefly and allowed to equilibrate for 10 min. A measure of the fraction of the BC dye bound to lipid A (occupancy, Y) was calculated as  $Y = (F_0 - F) / (F_0 - F_{\text{max}})$ , where  $F_0$  is the fluorescence emission intensity of the BC solution alone,  $F_{\text{max}}$  is the intensity in the presence of lipid A at the saturation concentration of the latter, and  $F$  is the fluorescence intensity of the BC/lipid A mixture at a given lipid A concentration. In the control experiments, independent occupancy measurements with PHMBG solutions were conducted in quadruplicate and a standard deviation was found to be approximately 5%. A Scatchard-type plot of the binding of BC to lipid A was plotted and yielded a dissociation constant  $K_d$ =0.344  $\mu$ M. In addition, LPS binding was tested to rule out the incidence of steric hindrance in the interaction with lipid A (which is a component of LPS). It was found that PHMBG could displace the BC dye from LPS almost as efficiently as PMB.

#### DNA binding by magnetic particles

Double-stranded  $\lambda$ DNA was used for quantification of DNA binding to the particles with the aid of a PicoGreen dsDNA Quantitation Reagent (Molecular Probes, Inc., a division of Invitrogen) according to the manufacturer's protocol. In brief, on the day of the experiment, an aqueous working solution of the PicoGreen dye was prepared by diluting the dye into 10 mM Tris-HCl, 1 mM EDTA buffer (pH 7.5, TE). Isotherms of DNA adsorption were measured by equilibrating a known concentration of DNA ( $C_0$ , M) with a suspension (1.0 mg/mL) of the particles in a mixture of a known volume ( $V$ , L) and particle content ( $m$ , g). A suspension of magnetic particles (1.0 mg/mL, 50  $\mu$ L) was mixed with 20 to 900  $\mu$ L of 2.0  $\mu$ g/mL DNA solution in TE buffer (pH 7.5) and the mixture in a centrifuge tube was vortexed briefly and kept at 25°C for 1 h while shaking. Equilibration for 0.75 and 8 h yielded equal results, within experimental error (estimated to be 15%), and thus 1 h appeared to be sufficient for reaching equilibrium. The particles were removed by centrifugation (15,000 g, 5 min) and the supernatant (20  $\mu$ L) was placed into wells of a 96-well microplate (Beckman Coulter). Control experiments were conducted to validate the particle and adsorbed DNA removal. Iron or cobalt concentration before and after centrifugation was measured using elemental analysis. Less than 1-2 wt% of total iron and less than 1 wt% of cobalt (relative to initial 1 mg/mL particle suspension) was left in the supernatant after centrifugation. Additionally,  $\lambda$ DNA solutions were centrifuged without particles under identical conditions and DNA concentration was measured using the PicoGreen Reagent. No measurable depletion of the DNA concentration was observed as a result of centrifugation without the particles. The separated supernatant was analyzed by adding a stock solution of PicoGreen into each well and quantifying DNA concentration in the supernatant ( $C_{\text{eq}}$ , M) using a fluorescence microplate reader (DTX 800 Multimode Detector, Beckman Coulter; excitation, 485 nm, emission, 535 nm). Calibration curves were prepared using 2  $\mu$ g/mL DNA stock solution as described in Beckman application notes. The concentration of the DNA adsorbed by the nanoparticles ( $\Gamma$ , mol/g) was determined by the relation  $\Gamma = (C_0 - C_{\text{eq}})V/m$ .

#### Cell viability and growth

Cultures of E.coli W3110 (prototrophic derivative of K-12 strain, ATCC 27325) were maintained on a minimal medium containing mineral salts, glucose, and agar at 37°C with aeration as described in detail elsewhere. The final cell batch was grown from a diluted ( $2 \times 10^8$  cells/mL) overnight culture. Then the cells were concentrated 100-fold by centrifugation and resuspended in 100 mM Tris-HCl (pH 7.0) to obtain suspensions of  $2 \times 10^{11}$  cells/mL. Portions of the concentrated suspensions were kept on ice overnight prior to testing. For long-term storage, liquid dispersions were mixed (1:1 v/v) with

sterile glycerol and stored at –80oC. The pH of the suspensions was adjusted to 7.0 at 37oC using 0.5 mM morpholinepropane sulfonic acid-Tris.

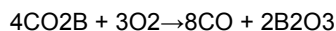
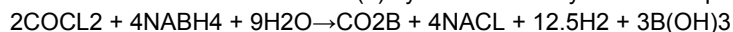
For the viability measurements, the cells (2 × 10<sup>9</sup> cells/mL) were preincubated for 10 min at 37°C in 50 mM Tris-HCl buffers, mixed with PMB solution or nanoparticle suspension in the same buffer for an additional 10 min, diluted with 0.9% NaCl, and dispersed on agar plates prepared with 1% peptone, 0.5% yeast extract, 1% NaCl, and 1.5% agar (pH 7.0) for the colony-forming units (cfu) determination. E.coli growth measurements were conducted in liquid cell suspensions grown in LB broth at 37oC while shaking at 200 rpm in sterile 200-mL glass flasks pre-treated with dimethyldichlorosilane as described previously.<sup>13</sup> Samples (2 mL) were withdrawn intermittently and the optical density at 650 nm (OD<sub>650</sub>) was measured spectrophotometrically in a stirred quartz cuvette (pathlength, 1 cm). The cell growth was expressed as 100x(OD<sub>650</sub> at time t minus OD<sub>650</sub> at the time just prior to the agent addition). All measurements were conducted in triplicate.

#### E.coli binding by magnetic particles

Suspensions of bacterial colonies (106-107 cfu/mL) were mixed, with brief vortexing, in a conical, 2-mL centrifuge tube containing 1 mL in 50 mM Tris-HCl buffer or PHMBG-PEI-M (t) nanoparticle suspension of known concentration in the same buffer. The nanoparticle suspensions were briefly sonicated just prior to the cell addition. The mixed suspensions were incubated at 37°C for 3 h with gentle shaking and the E.coli bound to the magnetic particles were separated by placing the tube on top of a 5x5x5 mm NdFeB, Grade N42 magnet (nominal surface field, 5754 Gauss, K&J Magnetics, Inc.), in a vertical position, for 0.5 h. The cells collected on the tube's bottom were concentrated by careful pipetting of the supernatant. The isolated NP-cell aggregates were washed with 50 mM Tris-HCl buffer (200  $\mu$ L×3), resuspended in 20 mL of the same buffer and subjected to the concentration determination by flow cytometry using bis-(1,3-dibutylbarbituric acid)trimethine oxonol (DiBAC4(3) stain, Molecular Probes, Inc., a division of Invitrogen) as described elsewhere. The same concentration determination assay was applied to the suspension of bacterial colonies just prior to their contact with the magnetic nanoparticles. The stain binds to both live and dead cells. The capture efficiency was calculated as follows: capture efficiency=100 x Count<sub>2</sub>/Count<sub>1</sub>, where Count<sub>1</sub> and Count<sub>2</sub> are the absolute cell counts/mL in samples before and after capture by magnetic nanoparticles; the Count values are adjusted for dilutions.

#### Particle Design and Properties

Magnetite particles were synthesized by the coprecipitation of iron (II) and (III) chlorides by ammonia, with branched polyethyleneimine (PEI) coating the particle core composed of magnetite. The PEI-functionalized magnetite particles (PEI-M) were further conjugated with PHMBG via linking of the amino-groups of PEI with the amino/imino groups of PHMBG by glutaraldehyde, resulting in the PHMBG chains being exposed to the exterior of the nanoparticle clusters. The chemistry and structure of the PHMBG-PEI-M particles have been discussed recently in more detail. The particles were characterized by a variety of methods. We observed that the particles in the initial dispersion prior to the HGMS process were quite polydisperse, with a significant fraction (approximately 20 wt%) in the range of 10-50 nm in size. By applying HGMS, the particles were fractionated to allow the particle size effects on the interaction of these particles with E.coli membranes and their effects on microorganism viability and growth to be investigated. Importantly, all the magnetite-based particle fractions possessed the same chemical composition. In addition, a new family of functionalized nanoparticles based on Co(0) modified with PHMBG was obtained via reduction of Co(II) by sodium borohydride in the presence of oxygen:



When the mixture is exposed to oxygen, a sacrificial reaction takes place whereby boron is oxidized while cobalt is reduced, resulting in the conversion of Co<sub>2</sub>B to Co(metal). Formation of water-soluble complexes between cobalt (II) chloride and biguanide hydrochloride is known to be through the displacement of two chloride atoms by bidentate biguanide; similar complexation can be expected between cobalt ions embedded in the surface of the metallic cobalt particle and PHMBG. Typical magnetization results with the PHMBG-PEI-M and PHMBG-Co particles indicated that both particle species were superparamagnetic, as indicated by the lack of hysteresis in the magnetization-field coordinates at 300 K. The saturation magnetizations calculated per gram of magnetite or metallic cobalt were 56 and 22 emu/g for PHMBG-PEI-M and PHMBG-Co particles, respectively. The smaller magnetization values for magnetite-containing particles relative to the bulk value of 92 emu/g for magnetite are due to the significant volume fraction of the polymers and the existence of a well-developed surface layer with reduced magnetization on the individual nanoparticles. In the case of nanocrystalline particles of metallic cobalt, a saturation magnetization as high as 187 emu/g has been reported, but was observed to decline dramatically upon oxidation on exposure to air and the interaction with chemicals such as amines, on the cluster surface. The ease of oxidation and atomic rearrangement in cobalt particles, which depend strongly on the presence of chemicals enabling colloidal stability, make PHMBG-Co a less likely candidate for potential biotechnology applications involving contact with microorganisms, relative to the magnetite-based particles. On the other hand, cobalt oxide nanoparticles have been found to enter human cell lines rapidly, remaining confined in vesicles inside the cytoplasm, and Co<sub>3</sub>O<sub>4</sub> and cobalt ions are known to impair cell viability. The reported bioactivity, along with the notion that both cobalt oxide and cobalt ion species are most likely situated on the surface of the polymer-chelated cobalt particles, motivated the inclusion of the PHMBG-Co species in the present study. The contents of magnetite and polymers in the particles were determined by thermogravimetric and elemental analysis, and are collected in Table 1, along with other important characteristics of the particles under study.

Table 1. Composition and physical properties of PHMBG-PEI-M and PHMBG-Co particles.

Parameter	PHMBG-PEI-M	PEI-Co
Fe <sub>3</sub> O <sub>4</sub> or Co content (%)	50.1	59.5



Polymer content (%)  
 PEI  
 PHMBG 49.9  
 24.3  
 25.6 40.5  
 0  
 40.5  
 Hydrodynamic diameter (nm)<sup>a</sup> 332 (total)  
 317 (large)  
 12 (small) 215  
 $\zeta$ -Potential (mV)<sup>b</sup> 38.9 $\pm$ 0.6 51.2 $\pm$ 0.8  
 Saturation magnetization<sup>c</sup> (emu/g) 56 22  
<sup>a</sup> Mean number-average, measured at pH 7.4  
<sup>b</sup> Measured at pH 7.4  
<sup>c</sup> Measured at 300 K

#### Nanoparticle binding to and magnetically directed manipulation of E.coli cells

The PHMBG-PEI-M (t) particles with the properties described above appeared to bind strongly to E.coli cells in buffered suspensions at pH 7.4, with capture efficiencies of approximately 65% and >99% using 0.2 and 2 mg/mL particle concentrations, respectively. The cells could not survive contact with and capture by the nanoparticles in these experiments (see Experimental). Our particles moved rapidly under strong magnetic fields and could be delivered to small areas where the bacteria had been located. E.coli were incubated in a Petri dish and allowed to adhere to the center of the bottom of the dish for 8 h. A strong NdFeB magnet (5x5x5 mm) was placed under the center of the Petri dish followed by the addition of PHMBG-PEI-M (t) particles. The resulting particle concentration was 0.1 wt%. With gentle agitation, the particles were attracted to the center of the Petri dish by the magnetic field, where they killed the bacteria. Analogous results on directed manipulation of silver-containing magnetic particles have been described previously. However, the antibacterial properties of the silver-containing particles stem from the silver ion dissociating from the particles and diffusing to the environment, and thus the efficiency of such particles depends on the loading level of the silver. As indicated by our cell-particle binding results, the PHMBG-modified particles kill bacteria on contact due to the strong association with their membranes. Our previous experiments with a variety of microorganisms have demonstrated a very small minimum inhibition concentration (MIC) of particles comparable to those of potent bactericides.

#### PHMBG and nanoparticle binding to lipid A

The interactions between our nanoparticles and lipid A were quantified by a highly sensitive fluorescent assay method developed for the screening of lipopolysaccharide-binding molecules. The derivative of cadaverine (BC) binds specifically to the lipid A portion of the lipopolysaccharide, mainly through salt-bridge interactions between the protonable group of cadaverine and the phosphates of the glycosidic portion of lipid A. The assay enables quantification of the competitive displacement of BC from its complex with lipid A by other LPS-binding species.

We used the BC-specific assay to analyze the binding of nanoparticles to the lipid A portion of the LPS. The addition of PHMBG solution or nanoparticle suspension results in a displacement of the BC probe, i.e., a decrease in the occupancy factor and consequently an increase in fluorescence. Polymyxin B (PMB), a decapeptide antibiotic and “gold standard” lipid A binder, was used as a positive reference control. Comparison of the BC-binding displacement curves indicates that PHMBG had an affinity to lipid A very similar to that of PMB, with the effective concentrations necessary for displacement of 50% of the bound fluorescent probe (ED50) found to be 0.51, 0.54, and 0.21  $\mu$ M for PMB, PHMBG, and PHMBG-PEI conjugate, respectively. This measured ED50 for PMB is close to that reported previously for the BC displacement assay. It is interesting to note that the number-average molecular weights of the two compounds are close (1300 Da for PMB and 1415 for PHMBG), so that their ED50 concentrations expressed in mass/volume units would be similar as well. ED50 values of 0.15, 0.15, 0.31, and 0.8  $\mu$ M were found for PHMBG-PEI-M (unfractionated, total), PHMBG-PEI-M(s) (average DH, 12 nm; devoid of large particles), PHMBG-PEI-M(l) (average DH, 317 nm; devoid of smaller-size fraction) and PHMBG-Co particles, respectively. The PHMBG-PEI-M species with a broad range of particle sizes as well as the fraction with the smaller PHMBG-PEI-M particles were about as effective (per weight/volume concentration basis) as PMB, PHMBG or the PHMBG-PEI conjugate in displacing the BC from its complex with lipid A. This is an indication that the PHMBG chains in these particles are located on the particle surface. Two-fold differences in ED50 observed between the unfractionated PHMBG-PEI-M particles and the fractionated species devoid of particles with hydrodynamic diameter below 50 nm could be explained by the presence of smaller particles in the unfractionated PHMBG-PEI-M with a high surface area-to-volume ratio, where the fraction of the biguanide and amine groups available for binding with lipid A on the particle surface is larger.

The presence of species with a high affinity binding to lipid A in the unfractionated PHMBG-PEI-M (t) and the smaller PHMBG-PEI-M (s) particles compared to that in the PHMBG-PEI-M (l) fraction shows that it is the smaller-sized particle fraction that binds lipid A with a high affinity exceeding that of the PMB standard. Overall, we have shown an efficient binding of the magnetic particles to lipid A, a part of the lipopolysaccharides involved in immune recognition by the Gram-negative bacteria

that, upon infection, activates the host immune system and is crucial in fighting pathogens. These results explain the efficiency with which these nanoparticles bind to and kill bacteria. Furthermore, as demonstrated above, facile binding of the paramagnetic particles to the microorganism membrane enables capture of the germ-particle complex by HGMS. As is evidenced by the high, positive  $\zeta$ -potential, the nanoparticles carry positive charges below the pKa of the amine/imine groups of the PHMBG and PEI (pH<11). The biguanide groups of the PHMBG are linked to the hydrophobic hexamethylene segments that are anchored in the hydrocarbon core of the fully saturated fatty acyl groups in each molecule of lipid A to create a low fluidity lipid interior of the PHMBG-lipid complex. When our particles are complexed with the E.coli membrane, the biguanide charge of the PHMBG is thus immobilized. The particle and membrane attract each other due to the attraction between the positive charge at the particle surface and the negative charges due to  $\alpha$ -glycosidic and non-glycosidic phosphoryl groups in the 1 and 4' positions of lipid A. The elastic stiffness of the membrane is much smaller than that of the particle, and thus the membrane has the potential to wrap around the particle to reduce the electrostatic energy. This can lead to rupture of the membrane and explain the observed bactericidal effect of the PHMBG-based particles.

#### Nanoparticle binding to DNA

A strong and cooperative binding between DNA and PHMBG prompted Allen et al. to imply that the bactericidal activity of PHMBG may be related to the interaction between the nucleic acids and PHMBG that penetrated into the cytoplasm. We have previously observed a considerable binding between plasmid DNA and PHMBG-modified, cationic magnetite nanoparticles, which led to the demonstration of selective capture of dissolved DNA from aquatic environment using HGMS. We quantified the binding between our paramagnetic nanoparticles and double-stranded DNA isolated from E.coli. Binding isotherms of  $\lambda$ -DNA (MW 3.15 MDa) and paramagnetic nanoparticles were measured at pH 7.5 and 20°C. All the particle species were strongly cationic at pH 7.5. The saturation binding capacities of the PHMBG-PEI-M (t), PHMBG-PEI-M (s), PHMBG-PEI-M (l), and PHMBG-Co particles were measured to be 270, 270, 240, and 300 pmol/g, respectively. One pmol of  $\lambda$ -DNA of 48.502 kb contains  $1.17 \times 10^{17}$  phosphate charges, whereas 1 g of PHMBG-PEI-PHMBG (t) contains up to approximately  $1.45 \times 10^{21}$  total positive charges, not accounting for a possible reduction in charge density due to the formation of Schiff base-links between PEI and PHMBG; the PHMBG-Co nanoparticles contain  $1.1 \times 10^{21}$  positive charges per gram. It appears, therefore, that at saturation, one phosphate group of DNA is bound to one in 40 to 50 of the cationic amino and/or biguanide groups on the nanoparticles. This finding suggests that the long, double-stranded molecules of  $\lambda$ -DNA coat the particle surfaces strongly, forming rigid polyelectrolyte complexes where the surface-bound cationic groups are sterically constrained and thus unable to pair with the phosphate groups.

#### Effect of nanoparticles on E.coli viability and cell growth

The particles under study exhibited dramatic bactericidal properties, with more than 99% of the E.coli cells being unable to form colonies after 10 min of incubation in a buffer containing 17.5  $\mu$ g/mL of any of the particle species. The effect of the PHMBG-PEI-M (s) and (t) species was very similar to that of the PHMBG solution, while PHMBG-Co particles were approximately 20% more effective at concentrations below 5  $\mu$ g/mL. Interestingly, the presence of small (<50 nm) PHMBG-PEI-M (s) particle species significantly impacted the effect of the particles on the cell viability, with the PHMBG-PEI-M (l) fraction devoid of small particles being 2 to 3-fold less efficient than the PHMBG-PEI-M (s) fraction in the particle concentration range 5 to 7.5  $\mu$ g/mL. This observation is in accord with the less efficient binding of the larger particles to the E.coli membranes represented by lipid A. Given the same chemical composition of these particles, the above observations suggest better accessibility of the cationic groups on the smaller particles for binding of the E.coli membranes due to the higher surface area/volume ratio. The growth characteristics of E.coli indicated analogous trends. At 5  $\mu$ g/mL, only PHMBG-Co completely inhibited the cell growth, whereas 3-4 h after addition of other species including PHMBG, the growth resumed. At 10  $\mu$ g/mL, all additives were bactericidal and inhibited the cell growth, except for the larger-size fraction of the PHMBG-PEI-M particles.

#### Conclusions: nanoparticle-bacteria binding

Since endocytosis is not characteristic of bacteria, they are unable to take up nanoparticles unless these particles penetrate through some damaged area of the bacterial membranes. This study demonstrated a new endotoxin- and DNA-binding species based on superparamagnetic nanoparticles functionalized with a membrane-damaging biguanide polymer, poly(hexamethylene biguanide). Polycationic properties and binding capacities of the particles for DNA are comparable to or exceed those of aminosilane-modified magnetic particles that are deemed feasible for applications involving DNA purification. Our particles are potent bactericides, which can be manipulated (separated and/or mechanically directed) by applying a magnet. This is of utility when a particle-bound germ needs to be captured for environmental monitoring or the particles are to be directed specifically to a location of germ colonies and biofilms, such as in water treatment systems and cooling devices and pipes. Such an ability to direct a biocide is unique to the paramagnetic species.

#### Utilization of montmorillonite materials for chemical protection

Montmorillonite K-10 functionalized with alpha-nucleophilic 2-pralidoxime (PAM) and its zwitterionic oximate form (PAMNa) is introduced as a versatile material for chemical protection against organophosphorous (OP) compounds such as pesticides and chemical warfare agents (CWA). Upon inclusion into the montmorillonite interlayer structure, the pyridinium group of PAMNa is strongly physisorbed onto acidic sites of the clay, leading to shrinking of the interplanar distance. Degradation of diethyl parathion by PAMNa-functionalized montmorillonite in aqueous-acetonitrile solutions occurred primarily via hydrolytic

conversion of parathion into diethylthio phosphoric acid, with the initial stages of hydrolysis observed to be pseudo-first order reactions. Hydrolysis catalyzed by the clay intercalated by PAMNa was 10- and 17-fold more rapid than corresponding spontaneous processes measured at 25 and 70°C, respectively. Hydrolytic degradation of diisopropyl fluorophosphate (DFP), a CWA simulant, was studied on montmorillonite clay functionalized by PAMNa and equilibrated with water vapor at 100% relative humidity by <sup>31</sup>P high-resolution magic angle spinning NMR and was observed to be rather facile compared with the untreated montmorillonite, which did not show any DFP hydrolysis within 24 h. The incorporation of the functionalized clay particles into elastomeric film of polyisobutylene was shown to be a means to impart DFP-degrading capability to the film, with clay particle content exceeding 18 wt%.

### **Technology Transfer**